

A Single Composition Architecture-Based Nanoprobe for Ratiometric Photoacoustic Imaging of Glutathione (GSH) in Living Mice

Chao Yin, Yufu Tang, Xiaozhen Li, Zhen Yang, Jie Li, Xiang Li, Wei Huang, and Quli Fan*

As one of the reduction species, glutathione (GSH) plays a tremendous role in regulating the homeostasis of redox state in living body. Accurate imaging of GSH in vivo is highly desired to provide a real-time visualization of physiological and pathological conditions while it is still a big challenge. Recently developed photoacoustic imaging (PAI) with high resolution and deep penetration characteristics is more promising for in vivo GSH detection. However, its application is dramatically limited by the difficult designation of photoacoustic probes with changeable near-infrared (NIR)-absorption under reductive activation. A cyanine derivative-based activatable probe is developed for in vivo ratiometric PAI of GSH for the first time. The probe is structurally designed to output ratiometric signals toward GSH in NIR-absorption region based on the cleavage of disulfide bond followed by a subsequent exchange between the secondary amine and sulfhydryl group formed. Such a ratiometric manner provides high signal-to-noise imaging of blood vessels and their surrounding areas in tumor. Concomitantly, it also exhibits good specificity toward GSH over other thiols. Furthermore, the single composition architecture of the probe effectively overcomes the leakage issue compared with traditional multicomposition architecture-based nanoprobe, thus enhancing the imaging accuracy and fidelity in living body.

Homeostasis of oxidation–reduction (redox) state in living body serves tremendous significance for maintaining the life of organisms.^[1] In such, biological oxidant and reductant are two predominant members that act as the “redox buffering” for regulating the redox balance.^[1b,2] Unfortunately, similar with generally referred oxidants of reactive oxygen species (ROS), aberrant generation of reductive biomolecules, especially glutathione (GSH), will perturb the redox balance and is closely related to various diseases including cancer, cardiovascular disease, aging, and Alzheimer’s disease.^[3] For example, GSH was reported to have much higher concentration in cancer cells (up to 1000-fold) compared with that in normal cells,^[4] making it one of the most

significant signal molecules to diagnose cancer. In virtue of its relatively high concentration and peculiar reductive property, development of activatable probes for GSH detection in vivo is highly desired to provide a real-time visualization of pathological conditions.^[5] Generally, these activatable probes are designed based on several mechanism of reaction with GSH, such as Michael addition,^[6] cleavage of sulfonamide and sulfonate esters,^[7] thiol–halogen nucleophilic substitution,^[8] and disulfide cleavage reaction.^[9] Among these, appropriate probes for ratiometric imaging are more promising to minimize the interference of complicated environmental factors in living body as they can provide a ratiometric signal output in two or more signal channels at a molecular level.^[10] Nevertheless, the ratiometric probes for in vivo GSH detection are rarely reported and mainly based on fluorescence mechanism that usually encounters the issues of shallow tissue-penetration depth and strong light scattering. To date, developing

ratiometric probes for GSH imaging in vivo with high resolution and fidelity is still a big challenge.

Photoacoustic imaging (PAI) is an emerging optical imaging technology that utilizes optical excitation and acoustic detection based on photoacoustic (PA) effect.^[11] It can overcome the high degree of scattering of optical photons in biological tissue and provide deeper imaging depth (up to 7 cm) and higher optical resolution,^[12] thereby effectively surmounting aforementioned constraints of fluorescence imaging. To date, several activatable probes based on near-infrared (NIR)-absorptive materials have been developed for in vivo PAI.^[13] However, only few ratiometric PA probes are reported for ROS,^[14] pH,^[15] and methylmercury^[16]

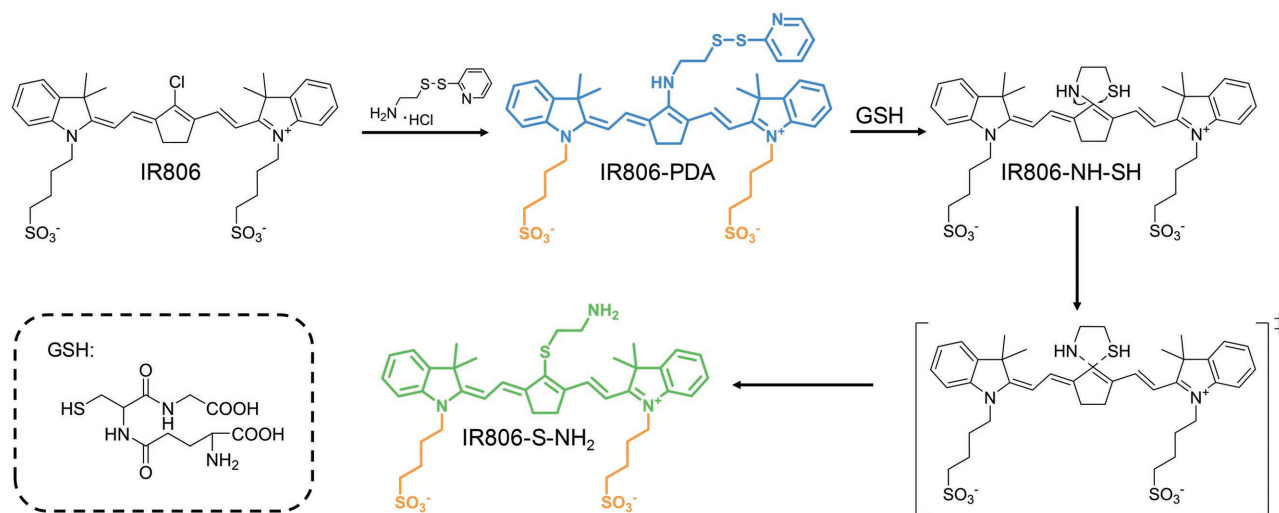
C. Yin, Y. Tang, X. Li, Z. Yang, J. Li, X. Li, Prof. W. Huang, Prof. Q. Fan
Key Laboratory for Organic Electronics and Information Displays
& Institute of Advanced Materials (IAM)
Jiangsu National Synergetic Innovation Center for
Advanced Materials (SICAM)
Nanjing University of Posts & Telecommunications
Nanjing 210023, China
E-mail: iamqlfan@njupt.edu.cn



The ORCID identification number(s) for the author(s) of this article can be found under <https://doi.org/10.1002/sml.201703400>.

DOI: 10.1002/sml.201703400

Prof. W. Huang
Shaanxi Institute of Flexible Electronics (SIFE)
Northwestern Polytechnical University (NPU)
Xi'an 710072, China
Prof. W. Huang
Key Laboratory of Flexible Electronics (KLOFE) & Institute of Advanced
Materials (IAM)
Jiangsu National Synergetic Innovation Center for Advanced Materials
(SICAM)
Nanjing Tech University (NanjingTech)
Nanjing 211816, China



Scheme 1. Synthesis procedure of IR806–PDA and the proposed pathways for the reaction of IR806–PDA with GSH. The disulfide bond of IR806–PDA can be cleaved by GSH and reductively evolved to sulfydryl group (–SH) to form the intermediate product (IR806–NH–SH). Then, a subsequent exchange between –SH and the secondary amine occurred to form the thiolate-substituted IR806 (IR806–S–NH₂).

imaging in living subjects. In such, there are two key limitations remained for concerning. On the one hand, most existing probes for ratiometric PAI are fabricated by integrating optically active components with high hydrophobicity into one entity via nanoprecipitation approach using amphiphilic block copolymers, thus inevitably undergoing the potential issues of slow dissociation as they are metastable micelles in nature.^[17] On the other hand, all reported probes for investigation of redox state are restricted to detect some oxidants, such as ONOO⁻ and ClO⁻,^[14] while those toward specific reductants, especially GSH, still remain a big challenge due to the difficult designation of probes with changeable NIR-absorption under reductive activation. Therefore, development of single composition architecture-based probes for in vivo ratiometric PAI of GSH is of great significance for evaluating the redox balance in living body.

In this study, the development of a cyanine derivative-based activatable probe, IR806-pyridine dithioethylamine (PDA), for ratiometric PAI of GSH in living mice was reported. IR806–PDA is constructed from the NIR-absorbing IR806 backbone whose active chlorine was substituted by amino group linked with a thiol-activatable side group, disulfide pyridine (–S–S–PDA). When treated with GSH, the disulfide bond can be cleaved and reductively evolve to sulfydryl group (–SH) with the extrusion of pyridine. Subsequently, the –SH further replaces the secondary amine to form the thiolate-substituted IR806 (IR806–S–NH₂) (**Scheme 1**). The remarkably different absorption properties of amino- and thiolate-substituted IR806 enable the real-time ratiometric PAI of GSH (**Figure 1**). Besides, such an amphiphilic nature endows the IR806–PDA probe with the ability to form homogenous nanoparticles via self-assembly process in aqueous solution, which could not only facilitate the probe to passively accumulate in tumor region with relatively high local concentration to enhance the PA brightness, but also effectively overcome the dissociation-induced issues such as changed optical properties and unreliable imaging results compared with the multicomposition architecture-based nanoprobe fabricated from nanoprecipitation. As a proof-of-concept,

ratiometric PAI on GSH in vivo was successfully performed using the xenograft tumor mouse model.

The chlorine of IR806 can be rapidly replaced by amino group of 2-(pyridin-2-yl)disulfanyl)ethan-1-amine hydrochloride in the presence of triethylamine via amino-halogen nucleophilic substitution, affording the target probe (IR806–PDA) (**Scheme 1**). The successful substitution was preliminary observed by the absorption evolution along with the solution color changes from green (IR806) to blue (IR806–PDA) (**Figure S3**, Supporting Information). Furthermore, matrix assisted laser desorption/ionization time-of-flight (MALDI-TOF) mass spectra showed the highest mass peak of IR806–PDA at 863.092 Da (**Figure S1b**, Supporting Information), which exhibited an increased molecular weight of 150.752 Da compared with that of IR806 (712.340 Da). In combination with the ¹H NMR result as shown in **Figure S1a** (Supporting Information), it clearly confirmed the successful synthesis of IR806–PDA probe. IR806–PDA could spontaneously self-assemble into nanoparticles when directly dissolved in aqueous solution. Transmission electron microscopy (TEM) reflected the spherical morphology for the probe (**Figure 2a**). Dynamic light scattering (DLS) exhibited the average hydrodynamic size of IR806–PDA nanoprobe at 25.9 ± 2.3 nm (**Figure 2b**), which is consistent with the TEM result. No obvious precipitation can be observed through centrifugation and the hydrodynamic size of IR806–PDA remained unchanged after storage for more than one month in aqueous solution (**Figure 2c**), reflecting the high structure stability for the nanoprobe mainly resulted from good water solubility provided by sulfonic acid group as well as strong π–π stacking between the hydrophobic backbones of IR806–PDA. In contrast, the multicomposition architecture-based nanoprobe fabricated from nanoprecipitation shows changed size distribution after storage for one month in the previous report, indicating its structure instability.^[11e] The average zeta potential of IR806–PDA nanoprobe was determined as –28.08 mV (**Figure S4**, Supporting Information). Photophysical property investigations indicated that the nanoprobe exhibited a strong absorption peak centered at 658 nm in phosphate-buffered

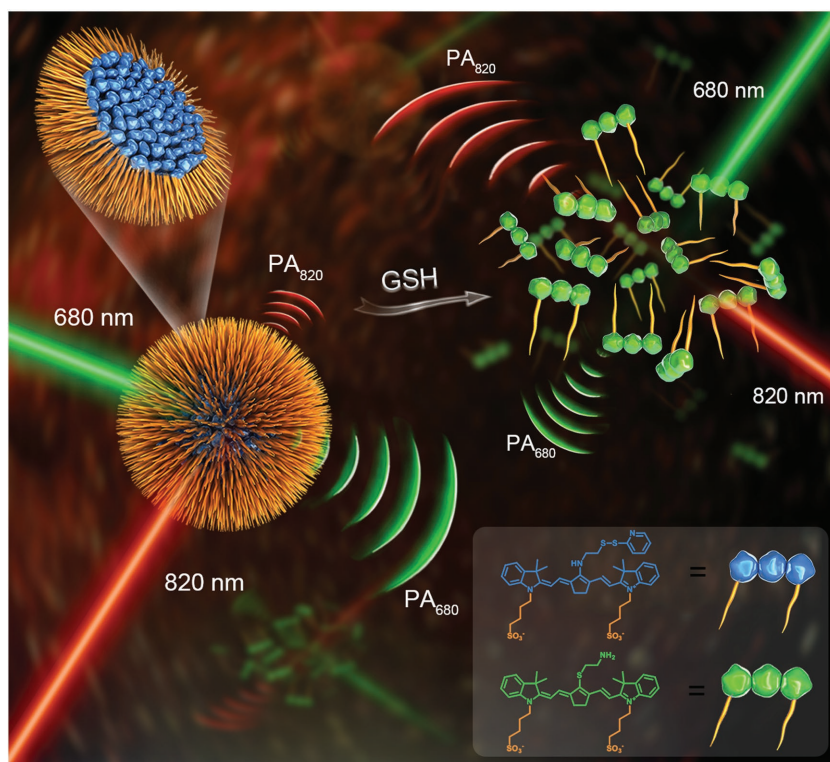


Figure 1. The illustration of IR806–PDA nanoprobe for ratiometric photoacoustic imaging of GSH. The PA intensity at 680 nm (PA_{680}) decreased while the PA signal at 820 nm (PA_{820}) enhanced upon activation by GSH.

saline (PBS) (pH = 7.4) with a high molar absorption coefficient of $2.48 \times 10^4 \text{ M}^{-1} \text{ cm}^{-1}$ (Figure S5, Supporting Information). Such a strong absorption ability reflected its high potential as an efficient NIR-absorbing contrast agent for PAI.

To investigate the optical responses of the IR806–PDA nanoprobe, changes in the absorption spectra of the nanoprobe toward various analytes were studied in PBS solution (pH = 7.4). The absorption peak at 658 nm gradually decreased, while a new absorption peak emerged at 820 nm and increased gradually with increased addition of GSH (Figure 2d). The sensing mechanism was validated by analyzing the molecular weight change of the nanoprobe before and after treatment of GSH (Figure S6a,b, Supporting Information). Accompanied with the disappearance of the molecular mass peak of the precursor at 863.092 Da, a new molecular mass peak at 754.011 Da was detected for GSH-treated nanoprobe. It confirmed that the disulfide bond of IR806–PDA was cleaved by GSH and reductively evolved to sulfhydryl group (–SH) to form IR806–NH–SH. In theory, given that the absorption backbone of the secondary amine-substituted IR806 is not damaged after the cleavage of disulfide bond, the product (IR806–NH–SH) will keep the pristine absorption peak at 658 nm. However, the observed new absorption peak at 820 nm, which significantly redshifted about 160 nm, demonstrated a new absorption backbone which was formed in our system after disulfide cleavage. Interestingly, we found that only a new molecular mass peak at 754.011 Da, which is the same as IR806–NH–SH, was detected (Figure S6b, Supporting Information) after disulfide

cleavage. Inspired by the phenomenon in previous report, which exhibited an inverse replacement of thiolate by amino in BODIPY-based probe,^[8] we thus proposed that a subsequent exchange between –SH and the secondary ammonium may occur to form the thiolate-substituted IR806 (IR806–S–NH₂) (Scheme 1) in our system. To further validate our conjecture, a thiolate-substituted IR806 (IR806–S–C₆) was synthesized as control, and its maximal absorption peak located at 820 nm consistent with the emerging peak of IR806–PDA nanoprobe activated by GSH (Figure S8, Supporting Information). All these results effectively confirmed the rationality of our proposed sensing mechanism of the nanoprobe toward GSH. Interestingly, the average particle size of the nanoprobe decreased significantly to $2.98 \pm 1.1 \text{ nm}$ (Figure S9, Supporting Information) after treatment by GSH, which should result from the molecular state for the obtained IR806–S–NH₂ in aqueous media as this structural evolution led to a decrease of hydrophobic portion and thus disturbing the initial hydrophilic–hydrophobic balance as well as changing the existing state of the probe in aqueous solution. Similar but not the same, the absorption profile of the nanoprobe exhibited relatively weak response when treated with cysteine (Cys) or homo-

cysteine (Hcy) compared with that of GSH (Figure S10, Supporting Information). MALDI-TOF mass spectra also showed differences between GSH- and Cys/Hcy-treated nanoprobe. Except for the characteristic peak at $\approx 754 \text{ Da}$ which is the same as GSH-treated nanoprobe, the additional mass peak at 873.294 Da (IR806–Cys) for Cys- or 887.439 Da (IR806–Hcy) for Hcy-treated nanoprobe was detected (Figure S6c,d, Supporting Information). This phenomenon can be explained by the fact that Cys or Hcy is more prone to substitute the pyridine group to form the substitution product of IR806–Cys or IR806–Hcy, thus prohibiting the subsequent exchange between –SH and the secondary amine and further weakening the responses of the nanoprobe toward these two thiols. All the data reflected the capability of the IR806–PDA nanoprobe not only for specifically detecting thiols from other analytes, but also for effectively differentiating GSH over Cys/Hcy. Considering that GSH has remarkably higher abundance (1×10^{-3} – $10 \times 10^{-3} \text{ M}$) than any other biothiols such as Cys (below $100 \times 10^{-6} \text{ M}$) under physiological conditions,^[18] the ratiometric responses of the nanoprobe were almost completely induced by GSH in biological system. Additionally, such optical changes of the nanoprobe are not sensitive to pH ranging from 5.0 to 9.0 as reflected by the pH-independent responses of the nanoprobe toward GSH, Cys, and Hcy (Figure S11, Supporting Information). This proved the capability of the nanoprobe to detect thiols in a wide range of pH in both physiological (pH 7.4)^[19] and some pathological conditions such as malignant tumor (pH 6.5–6.8)^[15a]. The ratiometric spectra change of the nanoprobe permitted

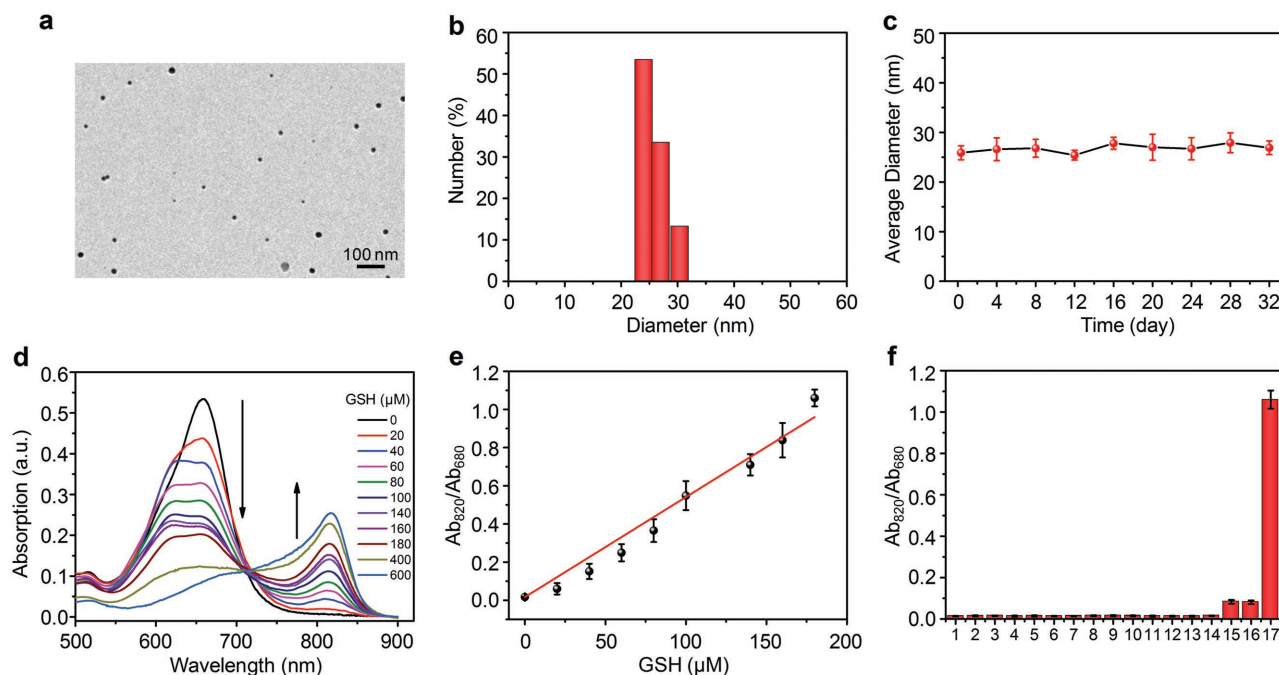


Figure 2. a) TEM image of the IR806–PDA nanoprobe. b) DLS result of the IR806–PDA nanoprobe. c) The average diameter fluctuation of the IR806–PDA nanoprobe stored in PBS for different time periods. d) UV–vis absorption spectra of the IR806–PDA nanoprobe (20×10^{-6} M) upon addition of GSH. e) Ratiometric absorption signals of the IR806–PDA nanoprobe (Ab_{820}/Ab_{680}) as a function of GSH concentration. The red line represents linear fitting from (GSH) = 0×10^{-6} – 180×10^{-6} M. f) The ratiometric absorption signals of the IR806–PDA nanoprobe (20×10^{-6} M) in the absence (1) or presence of different analytes (2, glycine (Gly); 3, glutamic (Glu); 4, valine (Val); 5, phenylalanine (Phe); 6, arginine (Arg); 7, tyrosine (Tyr); 8, serine (Ser); 9, histidine (His); 10, threonine (Thr); 11, proline (Pro); 12, tryptophan (Trp); 13, aspartate (Asp); 14, hydrogen sulfide (H_2S); 15, cysteine (Cys); 16, homocysteine (Hcy); 17, glutathione (GSH)) in $1 \times$ PBS (pH = 7.4). The concentration of all the analytes was fixed at 180×10^{-6} M (9 equiv.). The error bars represent the standard deviation of three separate measurements.

us to quantify signals using the absorption intensity ratio at 820 nm to that at 680 nm (Ab_{820}/Ab_{680}). A good linear correlation between the ratiometric absorption intensities (Ab_{820}/Ab_{680}) and GSH concentrations can be detected with the limit of detection (LOD) of 0.86×10^{-6} M (Figure 2e). At the optimized point (9 equiv. of thiols), the Ab_{820}/Ab_{680} value of GSH-treated nanoprobe reached 12.77- and 13.09-fold higher than that of Cys- and Hcy-treated nanoprobe, respectively (Figure 2f). The kinetics of thiols-induced optical change of the IR806–PDA nanoprobe was studied, reflecting that the nanoprobe can be almost completely activated by thiols within 25 min (Figure S12, Supporting Information). Considering the relatively high level of GSH in both cancer cells^[4] and tumor tissues^[20] compared with that in normal cells and tissues, the nanoprobe should have the capability to visualize upregulated GSH of tumor in living mice.

To validate the capability of the nanoprobe for PAI, ratiometric PAI of GSH using the nanoprobe was first demonstrated in solution. The PA spectrum of the nanoprobe ranging from 680 to 900 nm showed only one peak at 680 nm (Figure 3a), which was similar to the absorption spectrum of the nanoprobe in PBS (pH = 7.4) (Figure S3a, Supporting Information). Upon treatment with GSH, the PA signals of the nanoprobe from 680 nm gradually attenuated; whereas, a new peak at 820 nm emerged and remarkably increased (Figure 3a). The PAI of the nanoprobe solution incubated with GSH was further conducted at two wavelengths (680 and 820 nm), which were presented in

pseudo green and red, respectively. After addition of GSH to the nanoprobe solution, the green signals exhibited obvious attenuation compared with the control group; however, the red signals increased significantly (Figure 3c). Besides, the nanoprobe can also be activated by Cys or Hcy but showed weaker responses than GSH (Figure 3a,c), consistent with the absorption data. This double-channel PA response allowed us to perform ratiometric PAI of GSH. A good linear correlation between the ratiometric PA intensities (PA_{820}/PA_{680}) and the concentration of GSH was observed with the LOD of 3.13×10^{-6} M (Figure 3b), providing the probability for quantification of GSH using the nanoprobe. At the optimized point (9 equiv. of thiols), PA_{820}/PA_{680} of the nanoprobe treated by GSH reached 3.02- and 3.49-fold higher than that treated by Cys and Hcy, respectively (Figure 3d). In combination with its small size and low cytotoxicity as confirmed by MTT assay (Figure S13, Supporting Information), the nanoprobe should be an ideal candidate for in vivo PAI of GSH.

The application of the IR806–PDA nanoprobe for in vivo PAI of GSH was then examined using the subcutaneous Hela xenograft tumor model. The PA images from tumor region were recorded in two wavelengths at 680 and 820 nm, which were respectively presented in pseudo green and red (Figure 4a). The PA signals from blood vessels and their surrounding areas in the tumor can be vividly depicted due to the high imaging resolution of PAI. Relatively weak PA signal can be detected in the tumor before systemic administration of the nanoprobe due to

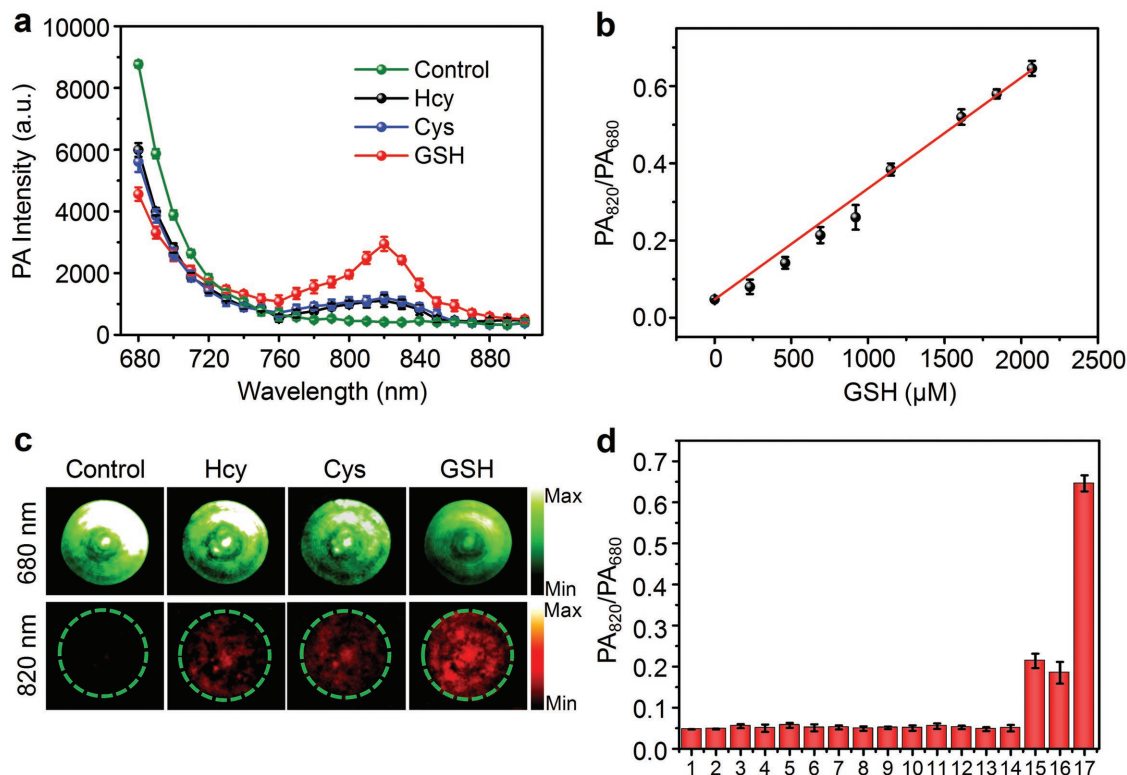


Figure 3. a) PA spectra of the IR806-PDA nanoprobe (230×10^{-6} M) in the absence (control) or presence of GSH, Cys, or Hcy at the concentration of 2.07×10^{-3} M (9 equiv.). b) Ratiometric PA signals of the IR806-PDA nanoprobe (PA_{820}/PA_{680}) as a function of GSH concentration. The red line represents linear fitting. c) PA images of the IR806-PDA nanoprobe in the absence (control) or presence of GSH, Cys, or Hcy. Signal collection was conducted under a pulsed laser turning to 680 or 820 nm. d) The ratiometric PA intensities of the IR806-PDA nanoprobe (230×10^{-6} M) in the absence (1) or presence of different analytes (2, Gly; 3, Glu; 4, Val; 5, Phe; 6, Arg; 7, Tyr; 8, Ser; 9, His; 10, Thr; 11, Pro; 12, Trp; 13, Asp; 14, H_2S ; 15, Cys; 16, Hcy; 17, GSH) in $1 \times$ PBS (pH = 7.4). The concentration of all the analytes was fixed at 2.07×10^{-3} M (9 equiv.). The error bars represent the standard deviation of three separate measurements.

the NIR-absorbing ability of oxy- and deoxy-hemoglobin in the blood (Figure 4a). In order to minimize the background interference, the PA intensity increment, ΔPA , which is defined as the difference value of the PA intensity after injection subtract that before injection of the nanoprobe, was employed to calculate the ratios of PA signal ($\Delta\text{PA}_{820}/\Delta\text{PA}_{680}$). ΔPA_{680} increased gently over time upon injection of the nanoprobe and reached the maximum at 1.5 h, whereas ΔPA_{820} exhibited a significant increase over time from 0 to 4 h and reached the plateau at 4 h postinjection (Figure 4b). The different evolution trends of the PA signals at 680 and 820 nm can be attributed to their different “accumulation-attenuation equilibrium” mechanisms: the strong signal increment at 820 nm should stem from the absorption increase at 820 nm due to the nanoprobe activation by GSH in the tumor microenvironment after accumulation via enhanced permeability and retention (EPR) effect due to its small size; whereas, the weak PA signal increase at 680 nm can be assigned to the synergistic effect of nanoprobe activation-induced PA signal decrease at 680 nm and nanoprobe accumulation in the tumor region. According to such signal changes in two channels, ratiometric PA signals ($\Delta\text{PA}_{820}/\Delta\text{PA}_{680}$) were calculated and showed gradual increase over time, which reached the maximum at 4 h postinjection (Figure 4c). At this time point, $\Delta\text{PA}_{820}/\Delta\text{PA}_{680}$ (0.53 ± 0.01) was ≈ 2.94 -fold higher than that at 0.5 h postinjection (0.18 ± 0.03). These results effectively proved

that the nanoprobe can be activated by GSH at tumor microenvironment and thus exhibited the practicability for ratiometric PAI of GSH in living body. Furthermore, we preliminarily investigated the pharmacokinetics of IR806-PDA nanoprobe by detecting its biodistribution in different organs including blood at 24, 36, and 48 h postinjection (Figure S14, Supporting Information). Results show that the PA intensity in tumor region at 24 h postinjection is higher than other organs except liver. The ideal biodistribution mainly resulted from the efficient EPR effect of IR806-PDA nanoprobe due to its proper size. At this time point, compared with other organs such as heart, spleen, and lung, liver shows the strongest PA signal, reflecting the predominant hepatobiliary clearance procedure of IR806-PDA nanoprobe which is quite similar to those for organic and inorganic nanoparticles with size higher than 10 nm.^[21] PA signals from all the organs indicated a gradual decrease after 24 h postinjection and almost vanished at 2 d postinjection.

In conclusion, we have designed and synthesized a cyanine derivative-based activatable nanoprobe (IR806-PDA) for in vivo ratiometric PAI of GSH. IR806-PDA was prepared through “one-step” nucleophilic substitution to introduce the disulfide pyridine (-S-S-PDA) side group into the backbone of IR806 dye. Such a molecular design not only endowed the probe with typical amphiphaticity to self-assemble into nanoparticles in biologically relevant solutions but also with highly

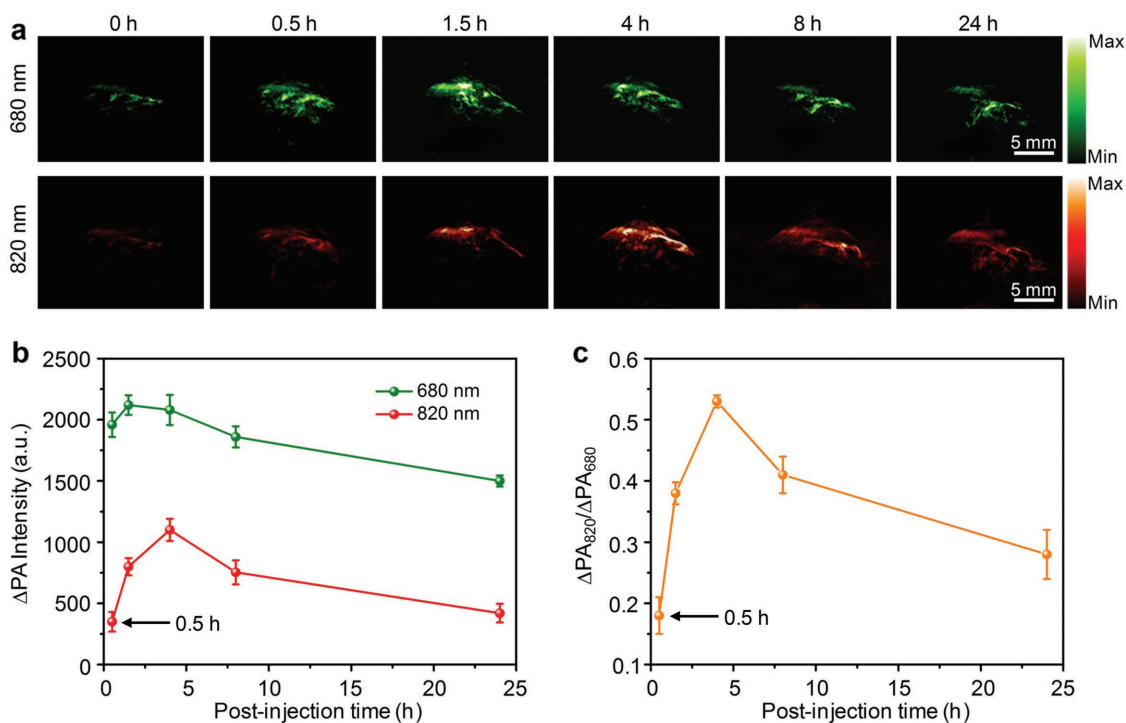


Figure 4. PAI of GSH in vivo. a) PA images of Helix tumor in a nude mouse before and after systemic administration of IR806–PDA nanoprobe (100 μg per mouse) for 0.5, 1.5, 4, 8, and 24 h. PA signal was collected under a pulsed laser turning to 680 or 820 nm. b) PA intensity increment in the tumor region at 680 (ΔPA₆₈₀) and 820 nm (ΔPA₈₂₀) as a function of postinjection time of the IR806–PDA nanoprobe. c) Ratiometric PA intensities (ΔPA₈₂₀/ΔPA₆₈₀) as a function of postinjection time. The error bars represent standard deviations of three separate measurements.

specific and sensitive optical responses toward GSH. More importantly, such single composition architecture of the nanoprobe effectively overcome the dissociation issue compared with the multicomposition architecture-based nanoprobe. In combination with its low cytotoxicity and small size, the nanoprobe was successfully conducted for in vivo ratiometric PAI of upregulated GSH in the tumor of living mice.

Our study thus developed a new generation of NIR-absorbing nanoprobe with single composition architecture for ratiometric PAI. The disulfide bond in our nanoprobe can be cleaved by high abundance of GSH in tumor environment for real-time PAI-visualized drug release for further theranostics when appropriate drugs are introduced into the nanoprobe through disulfide bond linkage. Furthermore, in view of the amphiphilic nature of the nanoprobe, it should have the potential to encapsulate other hydrophobic components such as imaging and sensing agents or drugs for multimodality imaging and imaging-guided therapy.

Supporting Information

Supporting Information is available from the Wiley Online Library or from the author.

Acknowledgements

C.Y. and Y.T. contributed equally to this work. This work was supported by the National Basic Research Program of China (No. 2012CB933301),

the National Natural Science Foundation of China (Nos. 21674048, 21574064, 61378081, 11404219, and 61505076), Synergetic Innovation Center for Organic Electronics and Information Displays, and the Natural Science Foundation of Jiangsu Province of China (Nos. BZ2010043, NY211003, and BM2012010).

Conflict of Interest

The authors declare no conflict of interest.

Keywords

glutathione, nanoparticles, NIR-absorption, photoacoustic imaging, self-assembly

Received: September 29, 2017

Revised: November 19, 2017

Published online:

- [1] a) H. M. Shapiro, *J. Surg. Res.* **1972**, *13*, 138; b) R. Kohen, A. Nyska, *Toxicol. Pathol.* **2002**, *30*, 620; c) B. Halliwell, *Plant Physiol.* **2006**, *141*, 312.
- [2] J. Hrbac, R. Kohen, *Drug Dev. Res.* **2000**, *50*, 516.
- [3] a) W. A. Kleinman, J. P. Richie, *Biochem. Pharmacol.* **2000**, *60*, 19; b) S. A. Lipton, Y. B. Choi, H. Takahashi, D. Zhang, W. Li, A. Godzik, L. A. Bankston, *Trends Neurosci.* **2002**, *25*, 474; c) S. M. Marino, V. N. Gladyshev, *J. Mol. Biol.* **2010**, *404*, 902; d) H. Refsum, P. M. Ueland, O. Nygard, S. E. Vollset, *Annu. Rev. Med.* **1998**, *49*, 31.

- [4] a) H. S. Jung, X. Chen, K. Seung, J. Yoon, *Chem. Soc. Rev.* **2013**, 42, 6019; b) S. C. Barranco, R. R. Perry, M. E. Durm, M. Quarishi, A. L. Werner, S. G. Gregorcyk, P. Kolm, *Dis. Colon Rectum* **2000**, 43, 1133.
- [5] a) Y. Yuan, R. T. K. Kwok, G. Feng, J. Liang, J. Geng, B. Z. Tang, B. Liu, *Chem. Commun.* **2014**, 50, 295; b) Q. Miao, C. Xie, X. Zhen, Y. Lyu, H. Duan, X. Liu, J. V. Jokerst, K. Pu, *Nat. Biotechnol.* **2017**, 35, 1102.
- [6] a) D. Kand, A. M. Kalle, S. J. Varma, P. Talukdar, *Chem. Commun.* **2012**, 48, 2722; b) H. Kwon, K. Lee, H. J. Kim, *Chem. Commun.* **2011**, 47, 1773.
- [7] I. S. Turan, F. P. Cakmak, D. C. Yildirim, R. Cetin-Atalay, E. U. Akkaya, *Chem. - Eur. J.* **2014**, 20, 16088.
- [8] L. Niu, Y. Guan, Y. Chen, L. Wu, C. Tung, Q. Yang, *J. Am. Chem. Soc.* **2012**, 134, 18928.
- [9] a) J. Li, C. Tian, Y. Yuan, Z. Yang, C. Yin, R. Jiang, W. Song, X. Li, X. Lu, L. Zhang, Q. Fan, W. Huang, *Macromolecules* **2015**, 48, 1017; b) G. Zeng, J. Li, H. Liang, Y. Yuan, X. Li, C. Yin, Z. Yang, Q. Fan, X. Lu, W. Huang, *Chin. J. Chem.* **2015**, 33, 881; c) B. C. Zhu, X. L. Zhang, Y. M. Li, P. F. Wang, H. Y. Zhang, X. Q. Zhuang, *Chem. Commun.* **2010**, 46, 5710.
- [10] S. Maruyama, K. Kikuchi, T. Hirano, Y. Urano, T. Nagano, *J. Am. Chem. Soc.* **2002**, 124, 10650.
- [11] a) Y. Jiang, P. K. Upputuri, C. Xie, Y. Lyu, L. Zhang, Q. Xiong, M. Pramanik, K. Pu, *Nano Lett.* **2017**, 17, 4964; b) Y. Jiang, K. Pu, *Small* **2017**, 13, 1700710; c) Z. Yang, R. Tian, J. Wu, Q. Fan, B. C. Yung, G. Niu, O. Jacobson, Z. Wang, G. Liu, G. Yu, W. Huang, J. Song, X. Chen, *ACS Nano* **2017**, 11, 4247; d) Q. Miao, K. Pu, *Bioconjugate Chem.* **2016**, 27, 2808; e) C. Yin, X. Zhen, H. Zhao, Y. Tang, Y. Ji, Y. Lyu, Q. Fan, W. Huang, K. Pu, *ACS Appl. Mater. Interfaces* **2017**, 9, 12332.
- [12] a) V. Ntziachristos, D. Razansky, *Chem. Rev.* **2010**, 110, 2783; b) L. H. V. Wang, S. Hu, *Science* **2012**, 335, 1458.
- [13] a) Y. Lyu, K. Pu, *Adv. Sci.* **2017**, 4, 1600481; b) Q. Chen, C. Liang, X. Sun, J. Chen, Z. Yang, H. Zhao, L. Feng, Z. Liu, *Proc. Natl. Acad. Sci. USA* **2017**, 114, 5343; c) L. Li, H. Ma, G. Qi, D. Zhang, F. Yu, Z. Hu, H. Wang, *Adv. Mater.* **2016**, 28, 254.
- [14] a) J. Zhang, X. Zhen, P. Upputuri, M. Pramanik, P. Chen, K. Pu, *Adv. Mater.* **2017**, 29, 1604764; b) C. Yin, X. Zhen, Q. Fan, W. Huang, K. Pu, *ACS Nano* **2017**, 11, 4174; c) K. Pu, A. J. Shuhendler, J. V. Jokerst, J. Mei, S. S. Gambhir, Z. Bao, J. Rao, *Nat. Nanotechnol.* **2014**, 9, 233.
- [15] a) Q. Miao, Y. Lyu, D. Ding, K. Pu, *Adv. Mater.* **2016**, 28, 3662; b) Q. Chen, X. Liu, J. Chen, J. Zeng, Z. Cheng, Z. Liu, *Adv. Mater.* **2015**, 27, 6820.
- [16] Y. Liu, S. Wang, Y. Ma, J. Lin, H. Y. Wang, Y. Gu, X. Chen, P. Huang, *Adv. Mater.* **2017**, 29, 1606129.
- [17] a) Z. L. Tyrrell, Y. Q. Shen, M. Radosz, *Prog. Polym. Sci.* **2010**, 35, 1128; b) X. Zhen, C. Zhang, C. Xie, Q. Miao, K. L. Lim, K. Pu, *ACS Nano* **2016**, 10, 6400.
- [18] X. Jiang, J. Chen, A. Bajić, C. Zhang, X. Song, S. L. Carroll, Z. L. Cai, M. Tang, M. Xue, N. Cheng, C. P. Schaaf, F. Li, K. R. MacKenzie, A. C. M. Ferreón, F. Xia, M. C. Wang, M. Maletić-Savatić, J. Wang, *Nat. Commun.* **2017**, 8, 16087.
- [19] A. Matsumoto, S. Ikeda, A. Harada, K. Kataoka, *Biomacromolecules* **2003**, 4, 1410.
- [20] a) P. Kuppusamy, H. Q. Li, G. Ilangovan, A. J. Cardounel, J. L. Zweier, K. Yamada, M. C. Krishna, J. B. Mitchell, *Cancer Res.* **2002**, 62, 307; b) R. Cheng, F. Feng, F. Meng, C. Deng, J. Feijen, Z. Zhong, *J. Controlled Release* **2011**, 152, 2; c) F. H. Meng, W. E. Hennink, Z. Zhong, *Biomaterials* **2009**, 30, 2180.
- [21] M. Longmire, P. L. Choyke, H. Kobayashi, *Nanomedicine* **2008**, 3, 703.